Nanotubes Hot Paper

International Edition: DOI: 10.1002/anie.201504349
German Edition: DOI: 10.1002/ange.201504349

General Formation of $M_xCo_{3-x}S_4$ (M = Ni, Mn, Zn) Hollow Tubular Structures for Hybrid Supercapacitors**

*Yu Ming Chen, Zhen Li, and Xiong Wen (David) Lou**

Abstract: *A simple and versatile method for general synthesis of uniform one-dimensional (1D) $M_xCo_{3-x}S_4$ (M = Ni, Mn, Zn) hollow tubular structures (HTSs), using soft polymeric nanofibers as a template, is described. Fibrous core–shell polymer@M-Co acetate hydroxide precursors with a controllable molar ratio of M/Co are first prepared, followed by a sulfidation process to obtain core–shell polymer@$M_xCo_{3-x}S_4$ composite nanofibers. The as-made $M_xCo_{3-x}S_4$ HTSs have a high surface area and exhibit exceptional electrochemical performance as electrode materials for hybrid supercapacitors. For example, the $MnCo_2S_4$ HTS electrode can deliver specific capacitance of 1094 $F g^{-1}$ at 10 $A g^{-1}$, and the cycling stability is remarkable, with only about 6 % loss over 20000 cycles.*

Metal sulfides, including binary and mixed-metal sulfides, represent a unique class of important multifunctional materials which can be used in many applications such as electrocatalysts for hydrogen evolution reactions, electrode materials for lithium-ion/sodium-ion batteries, and hybrid supercapacitors (HSCs).[1,2] Among these metal sulfides, considerable attention has been paid to ternary Ni-Co sulfides as promising electrode materials for HSCs.[3,4] In addition, the band gap of Ni-Co sulfides is lower than that of their counterparts, ternary Ni-Co oxides, thus suggesting the higher conductivity of Ni-Co sulfides.[4]

Hollow micro-/nanostructures are of great interest as a unique family of functional materials with well-defined interior voids and functional shells.[5] Their unique structural merits include large surface area, high pore volume, and low density, thus endowing them with the potential to be used in many fields, including catalysis, gas sensors, energy conversion, and storage systems.[6–12] As a result, there has been an increasing demand for simple and controllable synthesis of hollow nanostructured materials.[13–15] In particular, one-dimensional (1D) hollow tubular structures (HTSs) have been considered as promising hollow structures. For example, we have recently used 1D carbon and copper nanofibers to synthesize HTSs of metal oxides with a designed composition.[16,17] However, it is challenging to extend these 1D templates to produce HTSs of metal sulfides for different applications.

Herein, we report a general approach for preparing uniform 1D HTSs of $M_xCo_{3-x}S_4$ (M = Ni, Mn, Zn) using a soft fibrous polymeric template of polyacrylonitrile (PAN). The synthetic approach to 1D HTSs of $M_xCo_{3-x}S_4$ is schematically shown in Figure 1 (experimental details are available in the Supporting Information). First, soft PAN nanofibers, for use as the template, are prepared by electrospinning, followed by a precipitation strategy to obtain uniform fibrous core–shell PAN@M-Co acetate hydroxide composite precursors with a controllable molar ratio of M/Co.[18] Second, the as-prepared precursors can be sulfidized into core–shell PAN@-$M_xCo_{3-x}S_4$ composite nanofibers. Third, PAN nanofibers can be easily dissolved in *N*,*N*-dimethylformamide (DMF) to obtain well-defined $M_xCo_{3-x}S_4$ HTSs. Compared with other templates, which are usually removed by dissolution in acid/base or calcination in air, this soft polymeric template has many important advantages, including uniform morphology, flexible structure, copious functional groups, and easy removal in a suitable solvent at relatively low temperature. Importantly, the obtained uniform $M_xCo_{3-x}S_4$ HTSs exhibit exceptional electrochemical properties when evaluated as electrode materials for HSCs.

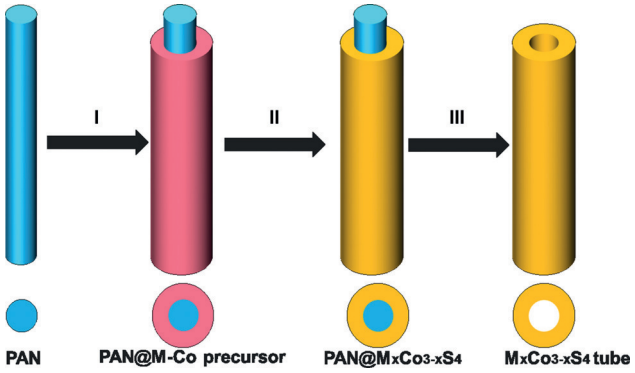

Figure 1. Schematic illustration of the formation of $M_xCo_{3-x}S_4$ nanotubes by using PAN nanofibers as soft templates: I) Growth process of M-Co precursors on PAN nanofibers. II) Solution sulfidation process. III) Removal of template in DMF.

Figure 2 shows the morphological characterizations of the PAN nanofibers and derived HTSs, by using $NiCo_2S_4$ as a typical example. As shown in Figure 2 a (see Figure S1 in the Supporting Information), uniform PAN nanofibers with a smooth surface and a diameter of about 200 nm can be

[*] Dr. Y. M. Chen, Dr. Z. Li, Prof. X. W. Lou
School of Chemical and Biomedical Engineering
Nanyang Technological University
62 Nanyang Drive, Singapore 637459 (Singapore)
E-mail: xwlou@ntu.edu.sg
davidlou88@gmail.com
Homepage: http://www.ntu.edu.sg/home/xwlou/

[**] The authors are grateful to the Ministry of Education (Singapore) for financial support through the AcRF Tier 2 funding (MOE2014-T2-1-058, ARC41/14; M4020223.120).

Supporting information for this article is available on the WWW under http://dx.doi.org/10.1002/anie.201504349.

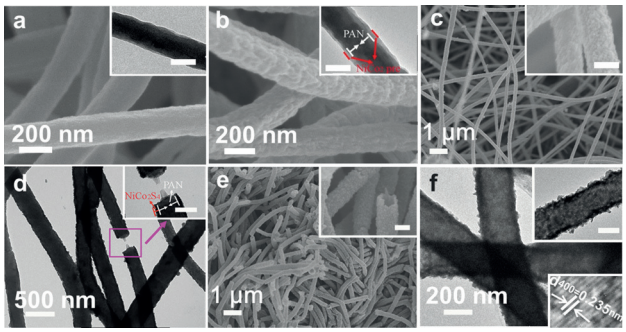

Figure 2. FESEM and TEM images of a) PAN nanofibers, b) the core–shell PAN@$NiCo_2$ precursor composite nanofibers, c,d) core–shell PAN@$NiCo_2S_4$ composite nanofibers, and e,f) $NiCo_2S_4$ HTSs. Scale bars in insets of (a–f) are 200 nm.

obtained by electrospinning. After refluxing, the surface of PAN nanofibers becomes rough (Figure 2b, and see Figure S2a in the Supporting Information), thus indicating the deposition of Ni-Co acetate hydroxide onto the PAN surface. The inset in Figure 2b shows a typical transmission electron microscopy (TEM) image of the PAN@Ni-Co precursor composite material, and it clearly shows the core–shell structure of the composite nanofibers with a larger fiber diameter of about 300 nm (see Figure S3 in the Supporting Information). The deposition of the precursor on the surface of PAN nanofibers is mainly due to the existence of functional groups (CN) within PAN nanofibers. The X-ray diffraction (XRD; see Figure S4 in the Supporting Information) pattern of the prepared precursors shows a tetragonal Ni-Co acetate hydroxide phase. After sulfidation treatment in a thioacetamide (TAA) solution, the 1D morphology is perfectly retained as shown in Figure 2c. Furthermore, a well-defined core–shell structure of PAN@$NiCo_2S_4$ can still be observed (Figure 2d), thus suggesting that the PAN core can maintain its structural integrity during the sulfidation process and growth of the $NiCo_2S_4$ shell. After treatment in DMF, the PAN core is completely removed to generate 1D HTSs with lengths of up to several micrometers, as revealed by the field-emission scanning electron microscopy (FESEM) image (Figure 2e). TEM studies clearly show the well-defined tubular structure with a shell thickness of about 50 nm (Figure 2f), which is consistent with FESEM observations. From the high-resolution TEM image (inset of Figure 2f), the resolved interplanar distance of 0.235 nm is ascribed to the (400) plane of $NiCo_2S_4$. XRD analysis shows that a heating treatment of the prepared materials under a nitrogen atmosphere increases the degree of crystallinity of the samples, thus yielding a pure $NiCo_2S_4$ phase of the products (JCPDS card no. 20-0782; see Figure S4). Energy-dispersive X-ray (EDX) results show that the Ni/Co atomic ratio of the synthesized $NiCo_2S_4$ HTSs is about 1:2.1, which is very close to the theoretical composition (see Figure S5 in the Supporting Information). The nitrogen sorption measurement suggests the existence of porous structures,[19] with pore sizes mostly below 20 nm (see Figure S6 in the Supporting Information), which gives rise to a high Brunauer-Emmett-Teller (BET) specific surface area of about 108.4 $m^2 g^{-1}$.

The relative Ni/Co composition in the Ni-Co acetate hydroxide can be easily altered by adjusting the molar ratio of Ni/Co in the starting materials (see Figure S2). After sulfidation (see Figure S7 in the Supporting Information), the corresponding HTSs of $Ni_xCo_{3-x}S_4$ (e.g., Ni_2CoS_4, CoS_x, and NiS_x) can be prepared as shown in Figure 3a,d (see also

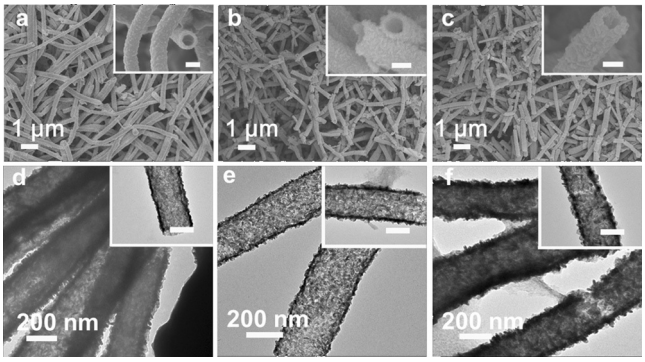

Figure 3. FESEM and TEM images of a,d) Ni_2CoS_4, b,e) $ZnCo_2S_4$, and c,f) $MnCo_2S_4$ HTS. Scale bars in insets of (a–f) are 200 nm.

Figure S8 in the Supporting Information). More importantly, this approach can also be extended to synthesizing HTSs of many other mixed-metal sulfides such as $ZnCo_2S_4$ (Figure 3b,e) and $MnCo_2S_4$ (Figure 3c,f) from their corresponding precursors (see Figures S9 and S10 in the Supporting Information). The composition of the as-made HTS is confirmed by EDX and XRD analysis (see Figures S11 and S12 in the Supporting Information). These results show that the present strategy is very effective, versatile, and general, and can be used to prepare HTSs of many functional mixed-metal sulfides, with controllable composition, for different applications.

These 1D HTSs of mixed-metal sulfides can find uses in many applications. Here we evaluate their promising application as electrodes for HSCs. Figure 4a shows typical cyclic voltammograms (CV) of $NiCo_2S_4$ and $MnCo_2S_4$ HTS electrodes at a scan rate of 2 $mV s^{-1}$ in a voltage window of 0 to 0.55 V versus a standard calomel electrode (SCE). It is clear that two distinct pairs of redox peaks can be seen in the CV curves. These well-defined peaks can be ascribed to the reversible Faradaic redox processes of MS/MSOH and MSOH/MSO.[4,20] Furthermore, in comparing two CV curves for $MnCo_2S_4$ and $NiCo_2S_4$, the first cathodic peak in the CV curves shifts to a more-negative potential when replacing Ni with Mn. As expected, the shift in the peak positions for both electrodes is also observed when increasing the sweep rate from 2 to 50 $mV s^{-1}$ (see Figures S13a and S14a in the Supporting Information). Figure 4b shows the galvanostatic charge/discharge voltage profiles in the potential range of 0–0.5 V at a current density of 5 $A g^{-1}$, with two distinct voltage plateaus in the charge and discharge processes for both electrodes, and they are in good agreement with the CV results. In principle, it might be more appropriate to report the charge stored in such battery-type electrodes as specific capacities.[21] For easy comparison with numerous works reported in recent literature, we present the data as specific

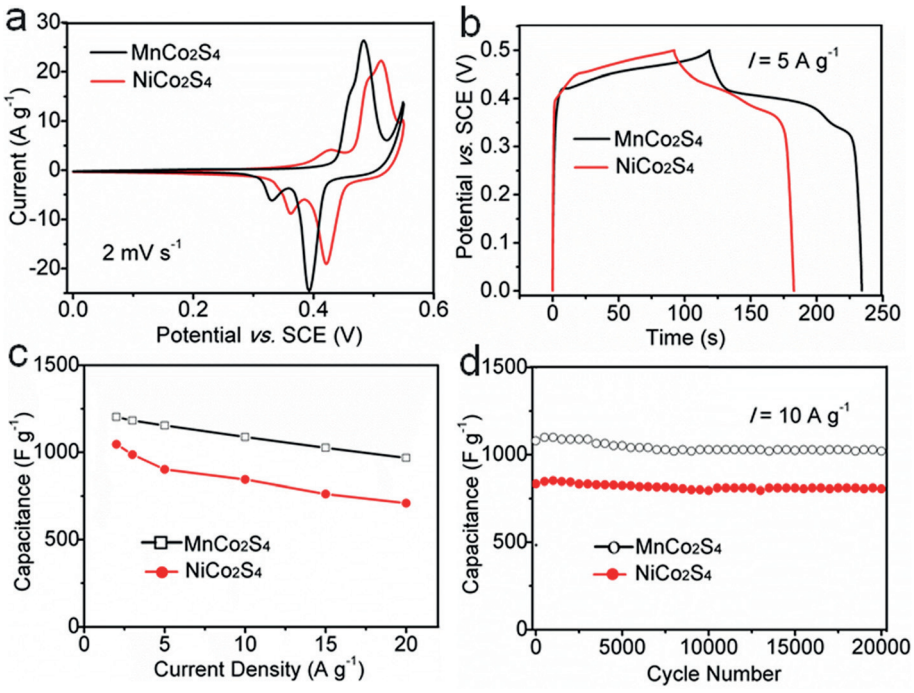

Figure 4. Electrochemical properties of $NiCo_2S_4$ and $MnCo_2S_4$ HTSs: a) CV curves at 2 $mV s^{-1}$. b) Charge-discharge voltage profiles. c) Specific capacitance at different current densities. d) Cycling performance at a current density of 10 $A g^{-1}$.

capacitance. The specific capacitance is obtained from chronopotentiometry (CP) curves of the $M_xCo_{3-x}S_4$ samples.

As seen in Figure 4c, the $NiCo_2S_4$ HTS shows a high capacitance of 1046, 987, 902, 844, 762, and 710 $F g^{-1}$ at different current densities of 2, 3, 5, 10, 15, and 20 $A g^{-1}$, respectively. This measurement corresponds to 68% of capacitance retention with the increase of current density from 2 to 20 $A g^{-1}$. More impressively, the $MnCo_2S_4$ HTS delivers outstanding capacitance of 1203, 1182, 1154, 1088, and 1026 $F g^{-1}$ at 2, 3, 5, 10, and 15 $A g^{-1}$, respectively. Even at a relatively high current density of 20 $A g^{-1}$, a specific capacitance of 968 $F g^{-1}$, corresponding to about 80% of the value at 2 $A g^{-1}$, can still be obtained, thus showing the exceptional rate capability of the prepared $MnCo_2S_4$ HTS. Additionally, the cycling stability of these two electrodes at 5 and 10 $A g^{-1}$ was also evaluated as shown in Figure 4d (see also Figure S13c and S14c). Both $NiCo_2S_4$ and $MnCo_2S_4$ HTSs show highly stable cycling performance. For the $NiCo_2S_4$ HTS, the initial capacitance at 10 $A g^{-1}$ is about 913 $F g^{-1}$ with a capacitance loss of less than 6% after 20000 cycles. The capacitance of $MnCo_2S_4$ HTS is 1094 $F g^{-1}$ in the first cycle at 10 $A g^{-1}$ and it decreases to 1028 $F g^{-1}$ after 20000 cycles with capacitance retention of about 94%. The electrochemical performance of these HTS is superior to that of previously reported mixed-metal sulfides.[3,4,22–27] It is important to mention that HTSs of other mixed-metal sulfides, such as $ZnCo_2S_4$ and Ni_2CoS_4, also show excellent electrochemical performance (see Figures S15 and S16 in the Supporting Information). Furthermore, these mixed-metal sulfide HTSs show much enhanced electrochemical properties as compared to CoS_x and NiS_x HTSs (see Figure S17 and S18 in the Supporting Information). Additionally, the structural integrity of typical HTS of $NiCo_2S_4$ can still be retained after cycling (see Figure S19 in the Supporting Information). Such a desirable electrochemical performance of 1D $M_xCo_{3-x}S_4$ HTSs might be attributed to their unique structural and compositional characteristics. Specifically, the hollow tubular space could act as a reservoir for electrolytes, and the large surface area enables sufficient electrode/electrolyte interface for fast diffusion and reaction, thereby resulting in excellent rate capability.[28] The permeable thin walls provide sufficient electroactive sites for electrochemical reactions, thus achieving high electrochemical activity.[27] In addition, the 1D hollow tubular architecture would enhance the structural integrity upon cycling, thus leading to a long cycle life.[23]

In summary, we have developed a simple general method for synthesis of uniform 1D hollow tubular structures of $M_xCo_{3-x}S_4$ (M = Ni, Mn, Zn) using electrospun PAN nanofibers as a soft functional template. The as-prepared $M_xCo_{3-x}S_4$ HTSs show exceptional electrochemical performance as electrodes for hybrid supercapacitors. In particular, $MnCo_2S_4$ HTSs deliver an initial specific capacitance of 1094 $F g^{-1}$ at 10 $A g^{-1}$ with a capacitance retention of about 94% after 20000 cycles. If coupled with a suitable negative electrode, it is possible to fabricate a high-performance hybrid supercapacitor with energy density close to that of lithium-ion batteries.

Keywords: mixed metal sulfides · nanotubes · polymeric template · supercapacitors

How to cite: *Angew. Chem. Int. Ed.* **2015**, *54*, 10521–10524
Angew. Chem. **2015**, *127*, 10667–10670

[1] C. W. Kung, H. W. Chen, C. Y. Lin, K. C. Huang, R. Vittal, K. C. Ho, *ACS Nano* **2012**, *6*, 7016–7025.
[2] C. H. Lai, M. Y. Lu, L. J. Chen, *J. Mater. Chem.* **2012**, *22*, 19–30.
[3] S. J. Peng, L. L. Li, C. C. Li, H. T. Tan, R. Cai, H. Yu, S. Mhaisalkar, M. Srinivasan, S. Ramakrishna, Q. Y. Yan, *Chem. Commun.* **2013**, *49*, 10178–10180.
[4] H. C. Chen, J. J. Jiang, L. Zhang, H. Z. Wan, T. Qi, D. D. Xia, *Nanoscale* **2013**, *5*, 8879–8883.
[5] Y. D. Yin, R. M. Rioux, C. K. Erdonmez, S. Hughes, G. A. Somorjai, A. P. Alivisatos, *Science* **2004**, *304*, 711–714.
[6] X. L. Pan, Z. L. Fan, W. Chen, Y. J. Ding, H. Y. Luo, X. H. Bao, *Nat. Mater.* **2007**, *6*, 507–511.
[7] B. Y. Xia, H. B. Wu, X. Wang, X. W. Lou, *J. Am. Chem. Soc.* **2012**, *134*, 13934–13937.

[8] Y. F. Zhu, J. L. Shi, W. H. Shen, X. P. Dong, J. W. Feng, M. L. Ruan, Y. S. Li, *Angew. Chem. Int. Ed.* **2005**, *44*, 5083 – 5087; *Angew. Chem.* **2005**, *117*, 5213 – 5217.
[9] J. Liu, S. Z. Qiao, J. S. Chen, X. W. Lou, X. R. Xing, G. Q. Lu, *Chem. Commun.* **2011**, *47*, 12578 – 12591.
[10] J. H. Lee, *Sens. Actuators B* **2009**, *140*, 319 – 336.
[11] K. T. Lee, Y. S. Jung, S. M. Oh, *J. Am. Chem. Soc.* **2003**, *125*, 5652 – 5653.
[12] L. Yu, H. B. Wu, X. W. Lou, *Adv. Mater.* **2013**, *25*, 2296 – 2300.
[13] M. Ibanez, A. Cabot, *Science* **2013**, *340*, 935 – 936.
[14] L. Zhang, H. B. Wu, X. W. Lou, *J. Am. Chem. Soc.* **2013**, *135*, 10664 – 10672.
[15] J. W. Nai, Y. Tian, X. Guan, L. Guo, *J. Am. Chem. Soc.* **2013**, *135*, 16082 – 16091.
[16] G. Zhang, B. Y. Xia, C. Xiao, L. Yu, X. Wang, Y. Xie, X. W. Lou, *Angew. Chem. Int. Ed.* **2013**, *52*, 8643 – 8647; *Angew. Chem.* **2013**, *125*, 8805 – 8809.
[17] H. Hu, L. Yu, X. Gao, Z. Lin, X. W. Lou, *Energy Environ. Sci.* **2015**, *8*, 1480 – 1483.
[18] W. Du, R. M. Liu, Y. W. Jiang, Q. Y. Lu, Y. Z. Fan, F. Gao, *J. Power Sources* **2013**, *227*, 101 – 105.
[19] Y. Chen, X. Li, K. Park, J. Song, J. Hong, L. Zhou, Y.-W. Mai, H. Huang, J. B. Goodenough, *J. Am. Chem. Soc.* **2013**, *135*, 16280 – 16283.
[20] L. Yu, G. Q. Zhang, C. Z. Yuan, X. W. Lou, *Chem. Commun.* **2013**, *49*, 137 – 139.
[21] T. Brousse, D. Bélanger, J. W. Long, *J. Electrochem. Soc.* **2015**, *162*, A5185 – A5189.
[22] T. Zhu, Z. Y. Wang, S. J. Ding, J. S. Chen, X. W. Lou, *RSC Adv.* **2011**, *1*, 397 – 400.
[23] L. Zhang, H. B. Wu, X. W. Lou, *Chem. Commun.* **2012**, *48*, 6912 – 6914.
[24] Z. S. Yang, C. Y. Chen, H. T. Chang, *J. Power Sources* **2011**, *196*, 7874 – 7877.
[25] W. J. Zhou, X. H. Cao, Z. Y. Zeng, W. H. Shi, Y. Y. Zhu, Q. Y. Yan, H. Liu, J. Y. Wang, H. Zhang, *Energy Environ. Sci.* **2013**, *6*, 2216 – 2221.
[26] Q. H. Wang, L. F. Jiao, H. M. Du, Y. C. Si, Y. J. Wang, H. T. Yuan, *J. Mater. Chem.* **2012**, *22*, 21387 – 21391.
[27] L. Yu, L. Zhang, H. B. Wu, X. W. Lou, *Angew. Chem. Int. Ed.* **2014**, *53*, 3711 – 3714; *Angew. Chem.* **2014**, *126*, 3785 – 3788.
[28] X.-Y. Yu, L. Yu, L. Shen, X. Song, H. Chen, X. W. Lou, *Adv. Funct. Mater.* **2014**, *24*, 7440 – 7446.

Received: May 13, 2015
Published online: July 14, 2015

